

## Hand Vein Pattern Recognition using Natural Image Statistics

T. Anantha Kumar\*, K. Premalatha, and A.M. Natarajan

Bannari Amman Institute of Technology, Sathyamangalam – 638 401, India

\*E-mail: anandmecse@gmail.com

### ABSTRACT

Biometrics is the science of identifying a person using physiological or behavioural characteristics. Hand vein pattern is a recent and unique biometric feature which is used for high secure authentication of individuals. The dorsal hand contains dorsal metacarpal veins, dorsal venous network, cephalic vein and basilic vein. This paper presents an image descriptor which uses statistical structure of natural images. In this work, stack of natural image patches are used as filters and these transform an image into integer labels describing the small-scale appearance of the image. These labels are converted into histogram and it is used for further image analysis. The feature space contains binarized statistical image features. The proposed work is tested on NCUT dataset with state-of-the-art algorithms. The experimental results demonstrate that the proposed work outperforms of the state-of-the-art algorithms with the recognition rate of 99.80 per cent.

**Keywords:** Biometrics, dorsal hand vein, natural image statistics, LBP, LPQ

### 1. INTRODUCTION

Personal verification is fundamental in any identity-based access control system and there is an increasing use of biometric features to authenticate individuals by measuring some inherent physiological or behaviour characteristics. Currently, a wide variety of applications require reliable verification schemes to confirm the identity of an individual, recognising humans based on their body characteristics has become more interesting in emerging technology applications.

#### 1.1 Biometric System

A biometric system is a technological system that uses information about a person to identify that person. Biometric systems rely on specific data about unique biological traits to work effectively. Biometric systems work by recording and comparing biometric characteristics, as shown in Fig. 1. When an individual first uses a biometric system, his identification features are extracted and enrolled as a reference for comparison in the future.

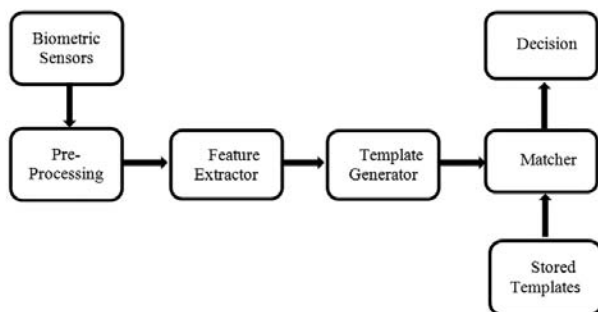


Figure 1. Working of a biometric system.

#### 1.2 Hand Dorsal Vein

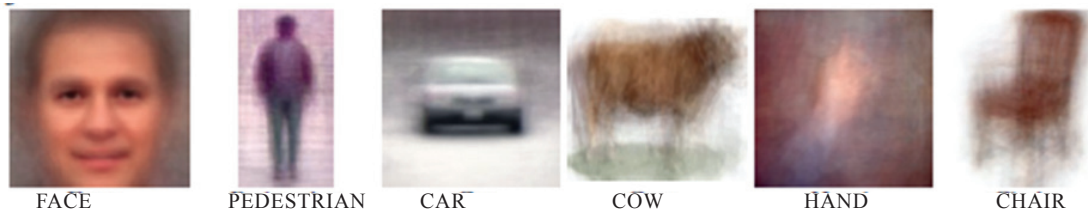
Vein pattern is the network of blood vessels beneath a person's skin. This vein pattern can be used to authenticate the identity of an individual. Veins are found below the skin and cannot be seen with naked eyes. Anatomically, apart from surgical intervention, the shape of the vascular patterns in the back of the hand is distinct from each other. Vein pattern is always the same, that is, the shape of the vein remains unchanged even when human being grows. Its uniqueness, stability, and immunity to forgery are attracting researchers. These features make it a more reliable biometric feature for personal identification. Furthermore, the state of skin, temperature, and humidity have little effect on the vein image, unlike fingerprint and facial feature acquirement. The hand vein biometrics principle is non-invasive in nature where dorsal hand vein pattern is used to verify the identity of an individual.

#### 1.3 Natural Image Statistics

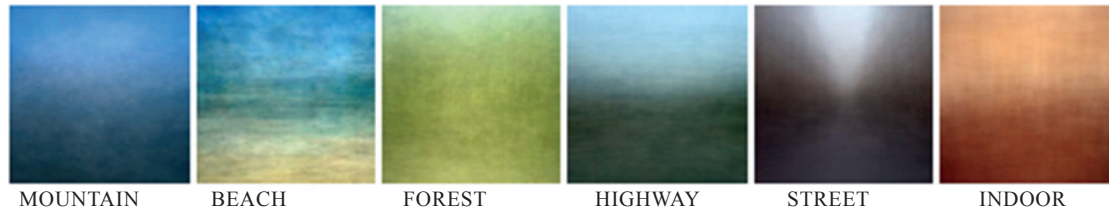
Natural images are photographs of the typical environment where people live. The statistical structure is described using a number of statistical models whose parameters are estimated from image samples. Figure 2 shows a collection of mean images created by averaging pictures from the same semantic category.

Natural image statistics deals with the statistical regularities related to the natural images. It is based on the foundation that a perceptual system is designed to natural images taken by individuals. Figure 3 shows the spectral signatures of 14 different image categories. Each spectral signature is obtained by averaging the power spectra of a few hundred images per category. The contour plots show the dominant spatial scales

OBJECTS



SCENES



OBJECTS IN SCENES



Figure 2. Averaged pictures of categories of images<sup>1</sup>.

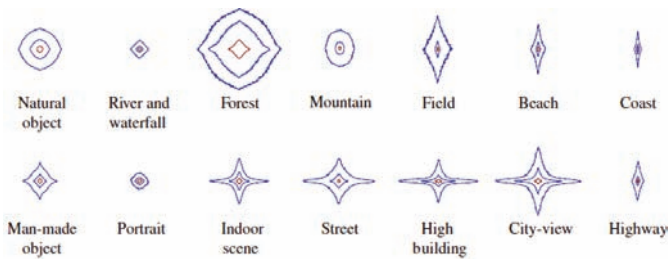


Figure 3. Spectral signatures of 14 different image categories<sup>1</sup>.

and dominant orientations for classes of scenes representing different volumes or depth ranges. The shape of the spectral signatures are correlated with the scale at which the main components of the image should be found. It gives an idea about statistics of natural image categories.

Natural image patches mean small sub-images (windows) taken at random locations in randomly selected natural images. For each input patch, one gets a realisation of that random variable. The natural image patches can be considered as a random vector. A set of more than 40,000 natural images can be obtained from [www.freefoto.com](http://www.freefoto.com) in which all images are taken with a range of different films, cameras, and lenses, and digitally scanned images. These are RGB colour images, spanning a range of indoor and outdoor scenes, JPEG compressed with an average quality of 90 per cent, and typically  $600 \times 400$  pixels. RGB images are converted into grayscale images and the random patches are chosen from the converted images. Figure 4 shows some natural image patches identified by Hyvarinen<sup>2</sup>, *et al.*

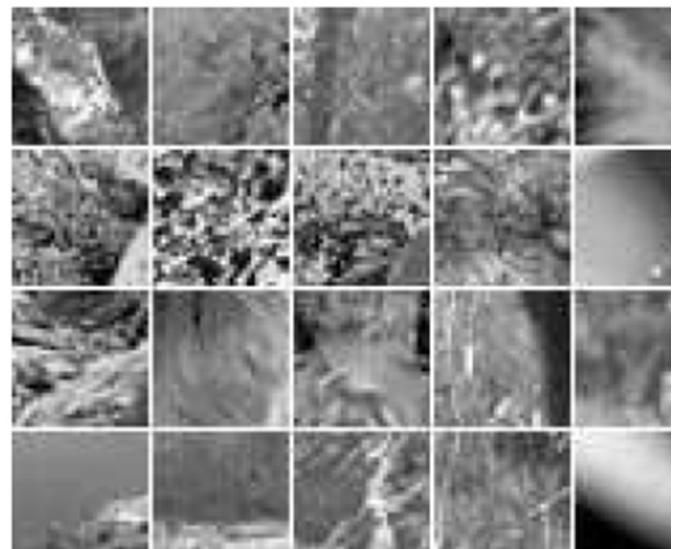


Figure 4 Some natural image patches<sup>2</sup>.

The proposed work adopts a local descriptor which was proposed by Kannala and Rahtu<sup>2</sup> for face recognition and texture classification. It automatically learns a fixed set of filters from a small set of natural images, instead of using handmade filters in local binary pattern and local phase quantisation. This approach is based on statistics of natural images and its modelling capacity.

2. HAND DORSAL VEIN DATASET

A dataset of 2040 hand vein images was acquired under

the natural lighting condition with a resolution of  $640 \times 480$ . It was named as North China University of Technology hand-dorsa vein dataset or NCUT dataset. In detail, 10 right and 10 left back of the hand vein images were captured from all 102 subjects, aged between 18 to 29 years, of which 50 were male while 52 were female.

The image coverage area is larger than the dorsal hand as shown in Fig. 5(a). In this work, the image centroid was identified to extract the ROI. Let  $(x_0, y_0)$  be the centroid of vein image  $f(x, y)$  then

$$x_0 = \frac{\sum_{i,j} i \times f(i, j)}{\sum_{i,j} f(i, j)} \quad (1)$$

$$y_0 = \frac{\sum_{i,j} j \times f(i, j)}{\sum_{i,j} f(i, j)} \quad (2)$$

Images were cropped wrt the centroid points in different sizes like  $320 \times 320$ ,  $340 \times 340$ ,  $360 \times 360$ ,  $380 \times 380$  and  $400 \times 400$  pixels. The cropped image of size  $360 \times 360$  pixels gives appropriate hand vein image and this size of images were taken for experimental analysis. Figure 5(a) shows back of the hand vein image captured with a resolution of  $640$  by  $480$ . Figure 5(b) and 5(c) respectively show the centroid and ROI of an image.

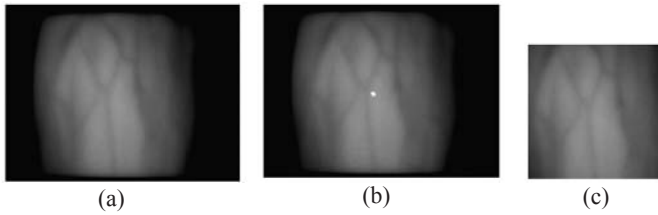


Figure 5. (a) Back of hand vein image, (b) Centroid, and (c) ROI.

### 3. IMAGE DESCRIPTOR USING NATURAL IMAGE STATISTICS

Most of the natural image statistical models are based on computing features. The features are used for any function of the image which will be used in further visual processing. The feature may be the output of the function or the computational operation which computes that value. One simple way of representing an image is a linear weighted sum of features.

Let each feature is denoted by  $A_i(x, y)$ ,  $i = 1, \dots, n$ . These features are assumed to be fixed. For each incoming image, the coefficient of each feature in an image is denoted by  $s_i$ . So the image  $I$  can be represented as follows

$$I(x, y) = \sum_{i=1}^n A_i(x, y) s_i \quad (3)$$

where  $I$  is an image,  $(x, y)$  is spatial coordinate in  $I$ ,  $A$  is a feature in image,  $s$  is a coefficient of a feature and  $n$  is the number of features. For simplicity, let one assumes that the number of features  $n$  equals the number of pixels then the system in Eqn. (3) is inverted as shown in the Eqn. (4). This means that for a

given image  $I$ , the coefficient  $s_i$  can be identified that fulfills this equation. This can be computed linearly as

$$s_i = \sum_{i=1}^n A_i(x, y) I(x, y) \quad (4)$$

There are many different sets of features that can be used like Fourier functions, wavelets, Gabor functions, features of discrete cosine transform, and many more. These sets attempt to represent all possible images, not just natural images, in a way which is optimal.

The most fundamental statistical properties of images are captured by the histograms of the outputs  $s_i$  of linear feature detectors. The output of a single linear feature detector with weights  $W(x, y)$  by  $s$  is denoted as follows in Eqn. (5)

$$s = \sum_{x, y} W(x, y) I(x, y) \quad (5)$$

where  $W$  is the weight and  $s$  is the single linear feature.

The statistics of the output contains more number of different histograms when the input of the detector consists of a large number of natural image patches. Thus, the feature  $s$  is a random variable, and for each input patch, to get a realisation of that random variable.

Kannala and Rahtu presented a method for constructing local texture descriptors, based on independent component analysis and efficient scalar quantisation scheme<sup>2</sup>. This feature tested with face images gives improved accuracy. The proposed work computes the binary code string for every pixel of a given image by natural image statistical filters. The code value of the pixel considers the local descriptor of an image intensity values in the pixel's neighbourhoods. The value of each bit binary code was calculated by binarising the response of linear filter with a threshold at 0. Each bit is related with different filters and the preferred length of the binary code decides the number of filters used. The set of filters is studied from a training set of natural image patches which increase the statistical independence of the filter response<sup>2</sup>. This statistical property of natural image patches decides the texture descriptor. Figure 6 shows the binary code string calculation using 12 filters of size  $3 \times 3$ .

In this paper, an image patch  $X$  was obtained from the numerical greyscale values of pixels in a patch of a natural image. A patch means a small sub-image or window. The patch size was taken as the size of the required filter. Image patches were randomly selected from the natural images. The random position and image selection were based on a random number generator implemented by the system.

Let  $X$  be an image patch of size  $l \times l$  and  $F_i$  be the linear filter of the same size. The filter response  $R_i$  is calculated by Eqn. (6).

$$R_i = \sum_{u, v} F_i(u, v) X(u, v) = F_i^T x \quad (6)$$

Given  $n$  linear filters  $F_i$ , stacks these to a matrix  $F$  of size  $n \times l^2$  and all responses are computed at once. The bit strings for all image patches of size  $l \times l$ , surrounding each pixel of an image, can be computed by  $n$  convolutions. The independence

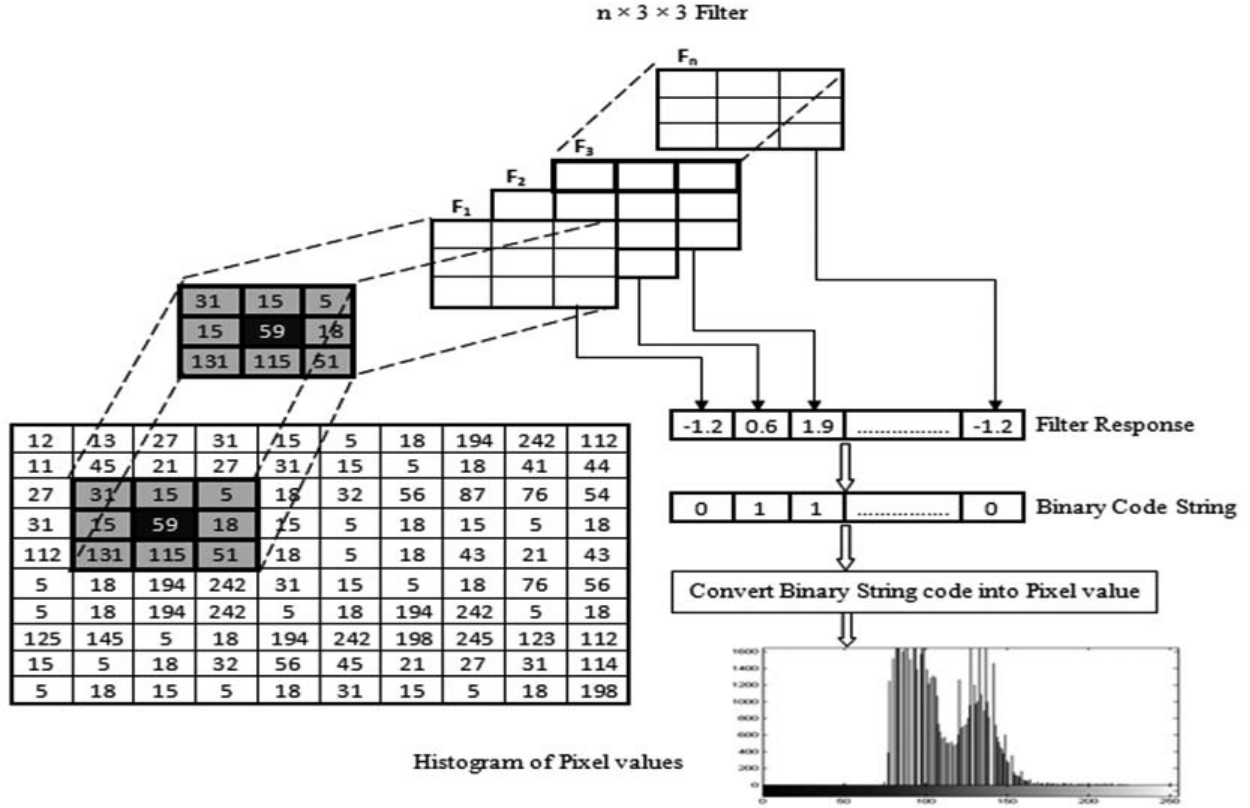


Figure 6. Binary code string calculation using set of filters.

of  $R_i$  provides justification for the proposed independent quantisation of the elements of the response vector  $R$ .

$$R = Fx \quad (7)$$

The filters  $F_i$  are determined by the natural image patches obtained from Hyvarinen<sup>2</sup>, *et al.* The elements of  $R_i$  of  $R$  are independent because the filters are determined by the natural image patches. The binary code string  $B$  for an image patch  $X$  is calculated by binarizing each element of  $R_i$  of  $R$  with a threshold at 0.

$$B_i = \begin{cases} 1 & \text{if } R_i > 0 \\ 0 & \text{otherwise} \end{cases} \quad (8)$$

where  $B_i$  is the  $i^{\text{th}}$  element of  $B$ .

The stack of  $n$  filters was applied for each pixel and the  $n$  bit binary code string  $B$  was calculated. The binary coded string is converted to a corresponding pixel value as

$$P_i = \sum_{j=1}^n B_i \times 2^j \quad (9)$$

#### 4. EXPERIMENT RESULTS ANALYSIS

In this section, the proposed method was assessed in NCUT hand vein dataset. The pattern matching was performed using nearest neighbour (NN) classifier. The NN is a commonly used classifier. An input sample is classified by calculating the distance to the training samples and the minimum of the results determine the classification of the sample. Histogram distance measures are used in NN classifier. The following distance measures was used to identify the distance between two histograms.

$$\text{Chi square : } \chi^2(p, q) = \sum_i \frac{(p_i - q_i)^2}{p_i + q_i}$$

$$\text{Cityblock distance : } d(p, q) = \sum_i |p_i - q_i|$$

$$\text{Euclidean distance : } d(p, q) = \sqrt{\sum_i (p_i - q_i)^2}$$

$$\text{Minkowski distance : } d(p, q) = \left( \sum_i |p_i - q_i|^k \right)^{\frac{1}{k}}$$

where  $k$  is assigned as 3 for Minkowski distance.

To obtain the filters  $F_i$ , the ideas were drawn from Hyvarinen<sup>2</sup>, *et al.*, and the filters are estimated by maximal statistical independence of  $B_i$ . The  $F$  was of size  $12 \times 17 \times 17$  where 12 represented the number of natural image patches and 17 represented filter size.

The biometric system generates two types of errors called the false rejection rate (FRR) and the false acceptance rate (FAR).

$$\text{FRR} = \frac{\text{No. of failed attempts at authentication by authorized users}}{\text{No. of attempts at authentication by authorized users}} \quad (10)$$

$$\text{FAR} = \frac{\text{No. of successful authentications by impostors}}{\text{No. of attempts at authentication by impostors}} \quad (11)$$

The recognition rate is given as

$$\text{Recognition rate} = \frac{\text{the number of recognized images}}{\text{the number of testing images}} \quad (12)$$

Both FAR and FRR depend on threshold. A higher threshold will generally reduce FAR, but at the expense of

increased FRR, and vice versa. The threshold affects FRR and FAR. At a low threshold, FRR will be low and FAR will be high.

Receiver operating characteristic (ROC) curve plots parametrically the FPR (100-specificity) on the x-axis, against the corresponding true positive rate (TPR) (sensitivity) on the y-axis as a function of the decision threshold. Each point on the ROC curve represents a sensitivity/specificity pair corresponding to a particular decision threshold. A test with perfect discrimination has a ROC curve that passes through the upper left corner (100% sensitivity, 100% specificity). Therefore, the closer the ROC curve is to the upper left corner, the higher is the overall accuracy of the test<sup>3</sup>.

Detection error trade-off (DET) curve (Martin<sup>23</sup>, *et al.*) plots error rates on both axes, giving uniform action to both types of errors. The DET curves can be used to plot matching error rates FRR against FAR and most of the image area used to highlight the differences of importance in the critical operating region.

The cumulative match curve (CMC) is used as a measure of 1:m identification system performance. It is used to discover the ranking capabilities of an identification system.

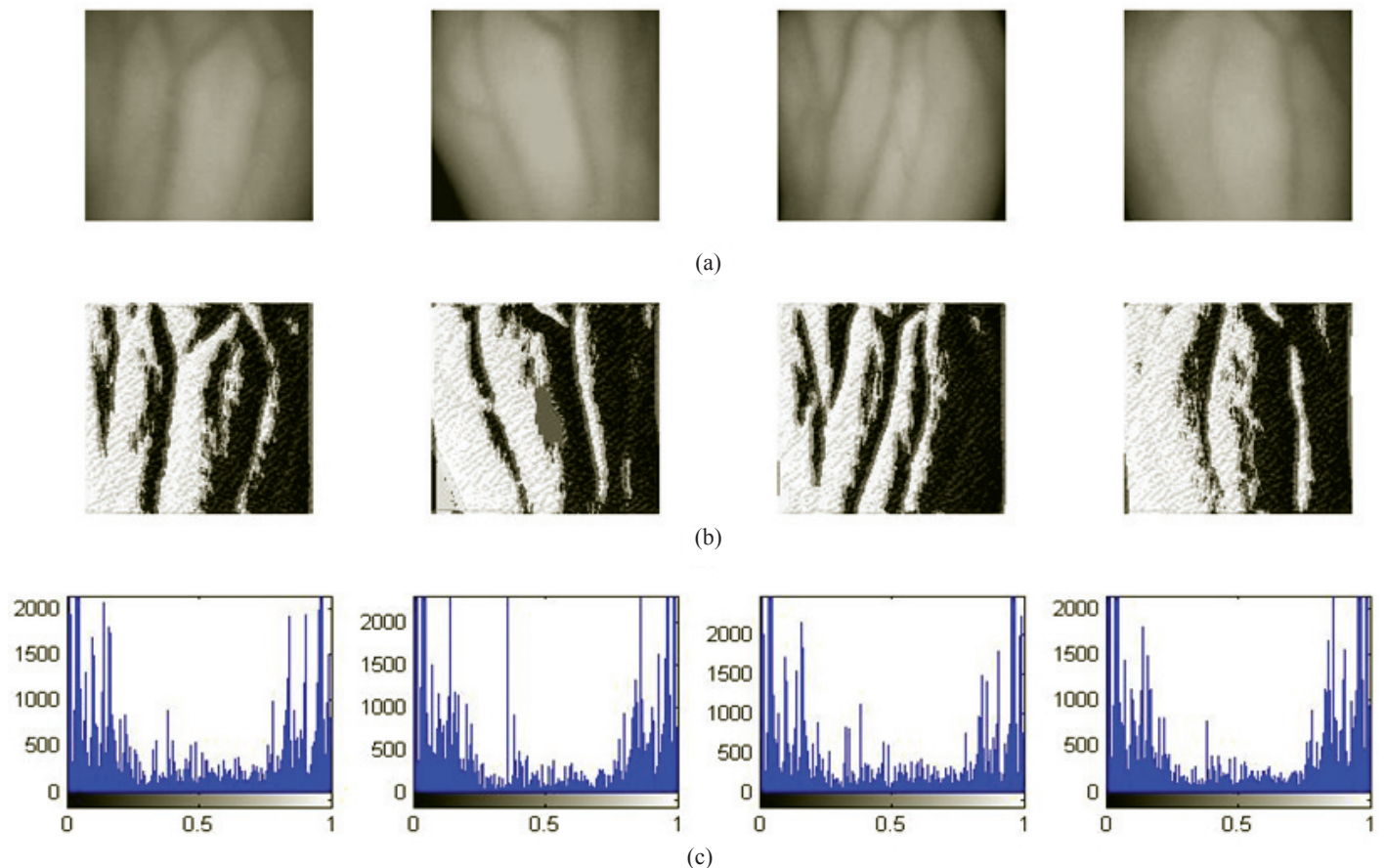
Table 1 shows description of NCUT hand vein dataset. Figure 7 shows some of the sample hand vein images from NCUT hand vein dataset and the corresponding code, and histogram obtained from natural image statistical descriptor.

Figure 8 shows ROC curve, DET curve, and CMC curve

**Table 1. NCUT dorsal hand vein data set**

Name of the databases	No. of subjects	No. of samples	Total no. of images	Size
NCUT hand vein database	102	20/subject (10 -Left and 10 -Right)	2040	640 × 480

obtained from the left hand dorsal vein for Euclidean, Cityblock, Minkowski and Chi-square measures. In receiver operating characteristic the more bowed is the curve towards the upper left corner, the better the classifier's ability to discriminate between the pattern classes. DET curve helps to indicate the performance of the system by plotting false match rate against the false non-match rate for a range of score thresholds. This will also estimate the widely used equal error rate (EER) which is the point at which the false match rate is equal to the false non-match rate. Figure 9 shows the EER obtained from Chi-square, Cityblock, Euclidean and Minkowski for left hand images. EER curve plots the FAR and the FRR on the vertical axis against the threshold score on the horizontal axis. The point of intersection of FAR and FRR curves is the EER, that is when the false acceptance rate is equal to the false rejection rate. Table 2 shows EER obtained from a left hand dorsal vein and right hand dorsal vein images. The Chi-square distance classifier gives the EER of 0.06 and this lowest EER value shows the higher the accuracy of the biometric system.



**Figure 7. A sample gallery of image and the corresponding natural image statistical descriptor code and histogram.**

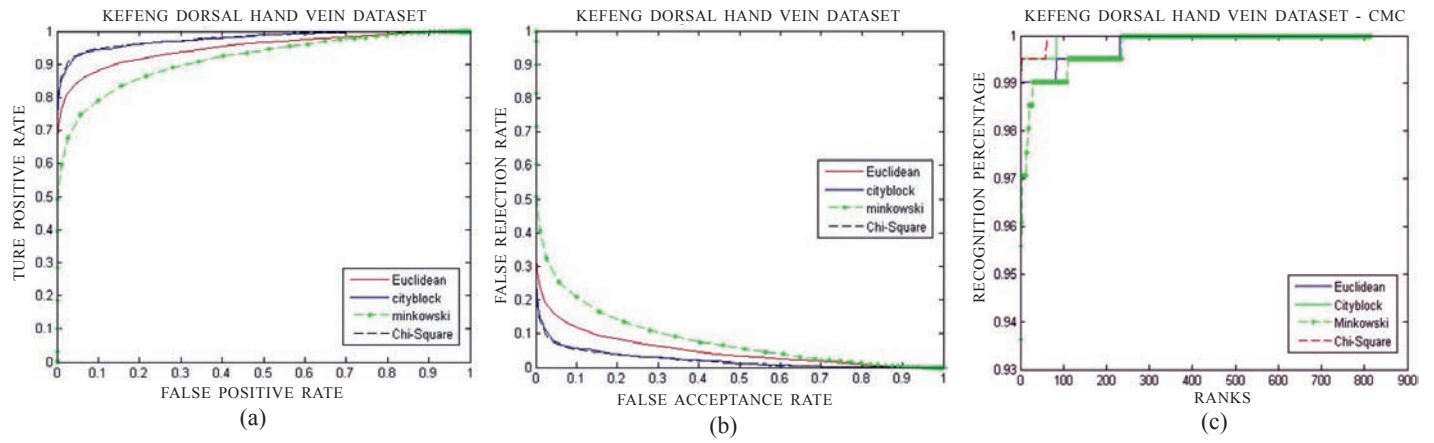


Figure 8. ROC, DET and CMC curve for Left hand images.

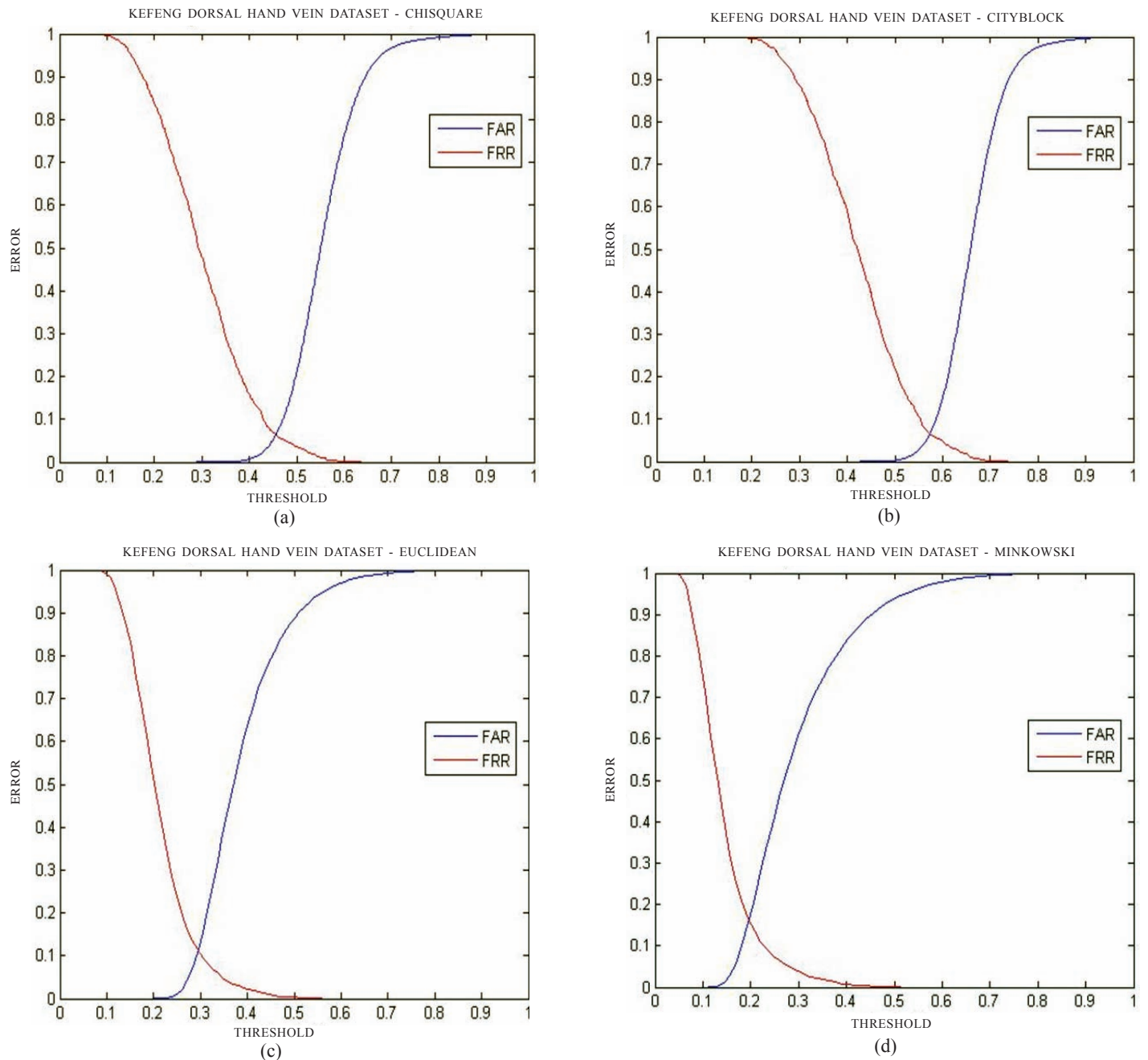


Figure 9. EER curves for left hand images.

Table 2 shows the EER of different methodologies for distinct hand dorsal vein images. The proposed work was analysed by varying the training samples from 1 to 9 and average recognition rate was calculated to check the performance of the system which is given in Table 3.

Evidently, as the number of training images was increased, the number of images available for test was decreased, and the recognition rate was improved and more time was required for computation.

Table 4 shows the comparison of recognition rates of proposed method using five-fold cross validation with state-of-the-art algorithms HOG, LBP, WLBP and LPQ for the NCUT data set and the proposed method outperforms the state-of-art methods.

Table 5 shows the performance of different methodologies for hand dorsal vein images.

**Table 2. Equal error rate**

Distance measure	Equal error rate	
	Left	Right
Chi-Square	0.05	0.06
Cityblock	0.06	0.07
Euclidean	0.15	0.12
Minkowski	0.18	0.15

**Table 3. Average recognition rate (%) of using different number of training images**

Training images/subject	Test images/subject	Chi-Square		Cityblock		Euclidean		Minkowski	
		Left hand	Right hand	Left hand	Right hand	Left hand	Right hand	Left hand	Right hand
1	9	86.89	88.45	86.67	88.87	67.18	78.43	51.20	66.41
2	8	94.24	93.87	93.01	93.75	83.57	87.86	70.09	78.30
3	7	96.91	96.49	96.21	96.07	88.93	91.03	76.33	83.61
4	6	98.36	98.85	98.52	98.69	92.48	94.77	83.82	88.72
5	5	98.82	99.01	98.62	99.01	94.51	96.27	87.45	90.78
6	4	99.51	99.26	99.26	99.26	97.05	98.28	90.19	94.60
7	3	99.51	99.26	99.34	99.44	98.03	99.34	93.79	95.49
8	2	99.51	99.51	99.75	99.80	99.16	99.34	97.59	98.48
9	1	99.75	99.75	99.80	99.80	99.51	99.34	98.52	98.85

**Table 4. Comparison of average recognition rates**

Distance measure	Chi - square		Cityblock		Euclidean		Minkowski	
	Left	Right	Left	Right	Left	Right	Left	Right
Methods	Average recognition rate (%)							
HOG	94.70	96.27	91.82	93.82	88.92	91.86	86.96	89.50
LBP	90.68	92.25	87.35	90.88	80.39	84.71	74.80	79.71
WLBP	94.79	96.07	93.32	92.05	79.21	50.80	68.03	39.20
LPQ	99.31	99.60	99.01	99.11	95.78	96.96	92.94	94.90
Proposed method	99.51	99.51	99.75	99.80	99.16	99.34	97.59	98.48

**5. CONCLUSION**

This paper explores a local image descriptor which is derived from stack of natural image patches that are statistically independent in filter response. It computes binary code for each pixel by linearly projecting the natural image patches on an image subspace and binarizes the coordinates via thresholding. The ROI of dorsal hand vein image is divided into  $17 \times 17$  overlapping rectangular regions and the 12 predefined filters learned from a small set of natural images are used. The binarized statistical image feature descriptor is computed independently within each of these regions. The kNN classifier is used with 5 fold cross validation to measure the recognition rate. The experimental results show that City block distance measure outperforms other distance measures with the recognition rate of 99.80%. Also the experiment results are examined with state-of-art algorithms HOG, LBP, WLBP and LPQ for the NCUT data set. It shows that the proposed work outperforms the existing state-of-art algorithms.

**ACKNOWLEDGEMENTS**

This work is supported by the research grant from Defence Research and Development Organization (DRDO), Government of India, New Delhi, grant no. ERIPR/ER/0903931/M/01/1321.

Portions of the research in this paper use the NCUT Hand-dorsa Vein Database collected by North China University of Technology, China.

**Table 5. Performance of different methodologies**

Reference	Methodology	Imaging	No. of subjects	Samples for each subject	Total images	Performance
Cross & Smith <sup>4</sup>	Sequential correlation in vein maps	NIR,HDF	20	5	100	FAR=0% FRR=7.9%
Kim <sup>5</sup> , <i>et al.</i> <sup>5</sup>	DSP processor	NIR imaging	Not mentioned	Not mentioned	5000	FAR=0.001% Reliability=99.45%
Tanaga & kubo <sup>6</sup>	FFT based phase correlation	NIR,HDF	25	Not mentioned	Not mentioned	FAR=0.073% FRR=4%
Fan <sup>7</sup> , <i>et al.</i>	Multi-resolution analysis and combination	Thermal hand vein imaging	32	30	960	FAR=3.5% FRR=1.5%
Wang & Leedham <sup>8</sup>	Line segment Housdorff distance matching	Thermal hand vein imaging	12	9	108	FAR=0% FRR=0%
Ding <sup>9</sup> , <i>et al.</i>	Distance between feature points	NIR imaging,	48	5	240	FAR=0% FRR=0.9%
Shahin <sup>10</sup> , <i>et al.</i>	fast spatial correlation	NIR imaging	50	10	500	EER=0.25%
Wang <sup>11</sup> , <i>et al.</i>	A multi-resolution wavelet algorithm	NIR imaging	82	10	820	FAR=0.046% FRR=5.08%
Wang <sup>12</sup> , <i>et al.</i>	Modified Hausdorff distance algorithm	Far-infrared imaging	47	3	141	EER=0%
Ajay Kumar & Prathyusha <sup>13</sup>	Vein triangulation and knuckle tips	NIR imaging	Not mentioned	Not mentioned	100	FAR=1.14% FRR=1.14%
Wang <sup>14</sup> , <i>et al.</i>	SIFT	NIR imaging	102	20	2040	FAR = 0.002% FRR = 0.93%.
Wang <sup>15</sup> , <i>et al.</i>	LBP	NIR imaging	102	20	2040	Recognition rate = 98.13%
Crisan <sup>16</sup> , <i>et al.</i>	Thinning algorithm	NIR imaging	306	2	612	FAR=0.012% FRR=1.03%
Huang <sup>17</sup> , <i>et al.</i>	Oriented Gradient Maps	NIR imaging	102	20	2040	Recognition rate = 97.60%
Wang and Liao <sup>18</sup>	LBP with back propagation encoder	NIR imaging	102	20	2040	Recognition rate = 97.60%
Wang <sup>19</sup> , <i>et al.</i>	Coded and weighted LBP	NIR imaging	102	20	2040	Recognition rate = 98.63%
Premalatha <sup>20</sup> , <i>et al.</i>	Local Gabor phase quantisation with whitening transformation	NIR imaging	102	20	2040	Recognition rate = 99.71%
Anantha kumar & Premalatha <sup>21</sup>	Local Gaussian quadrature filter pair phase quantisation	NIR imaging	102	20	2040	Recognition rate = 99.70%
This paper	Natural image statistical descriptor	NIR imaging	102	20	2040	Recognition rate = 99.80%

**REFERENCES**

1. Torralba, A. & Oliva, A. Statistics of natural image categories. *Network: Comput. Neural Syst.* 2003, **14**(3), 391-412. doi: 10.1088/0954-898X/14/3/302
2. Hyvarinen, A.; Hurri, J. & Hoyer, P.O. Natural image statistics: A probabilistic approach to early computational vision. Springer, England, 2009. pp. 448 doi: 10.1007/978-1-84882-491-1
3. Zweig, M.H. & Campbell, G. Receiver-operating characteristic (ROC) plots: a fundamental evaluation tool in clinical medicine. *Clinical Chemistry*, 1993, **39**(4), 561-577.
4. Cross, J.M. & Smith, C.L. Thermo graphic imaging of the subcutaneous vascular network of the back of the hand for biometric identification. *In Proceedings of the 29<sup>th</sup> Annual International Carnahan Conference on Security Technology.* Sanderstead, London, 1995.
5. Kim, S.; Park, H.M.; Kim, Y.W.; Han, S.C.; Kim, S.W. & Hang, C.H. A biometric identification system by extracting hand vein patterns. *J. Korean Phys. Soc.*, 2001, **38**(3), 268-272.
6. Tanaka, T. & Kubo, K. Biometric authentication by hand vein patterns. *In Proceedings of SICE Annual Conference: Yokohama, Japan, 2004.*
7. Fan, K.C. & Lin, C.L. Biometric verification using thermal images of palm-dorsa vein patterns. *IEEE Trans. Circuits Sys. Video Technol.*, 2004, **14**(2), 199-213. doi: 10.1109/TCSVT.2003.821975

8. Wang, L. & Leedham, C.G. A thermal vein pattern verification system. *In Proceedings of International Conference on Advances in Pattern Recognition*. Springer, Bath, UK, 2005. 58-65. doi: 10.1007/11552499\_7
9. Ding, Y.; Zhuang, D. & Wang, K. A study of hand vein recognition method. *In Proceedings of IEEE International Conference on Mechatronics & Automation*. Niagara Falls, Canada, 2005.
10. Shahin, M.; Badawi, A. & Kamel, M. Biometric authentication using fast correlation of near infrared hand vein patterns. *Int. J. Biomed. Sci.*, 2007, **2**(3), 141-148.
11. Wang, L.; Leedham, G. & Cho, D.S. Minutiae feature analysis for infrared hand vein pattern biometrics. *Pattern Recognit.* 2008, **41**(3), 920-929. doi: 10.1016/j.patcog.2007.07.012
12. Wang, Y.; Liu, T. & Jiang, J. A multi-resolution wavelet algorithm for hand vein pattern recognition. *Chin. Opt. Lett.*, 2008, **6**(9), 657 - 660. doi: 10.3788/COL20080609.0657
13. Ajay Kumar, K. & Prathyusha, K. Personal authentication using hand vein triangulation and Knuckle shape. *IEEE Trans. Image Process.*, 2009, **38**(9), 2127-2136. doi: 10.1109/TIP.2009.2023153
14. Wang, Y.; Wang, D.; Liu, T. & Li, X. Local SIFT analysis for hand vein pattern verification. *In Proceedings of the SPIE International Conference on Optical Instruments and Technology: Optoelectronic Information Security*. Shanghai, China, 2009.
15. Wang, Y.; Li, K. & Cui, J. Hand-dorsa vein recognition based on partition local binary pattern. *In Proceedings of 10<sup>th</sup> IEEE International Conference on Signal Processing: Beijing, China, 2010*. doi: 10.1109/ICOSP.2010.5656717
16. Crisan, S.; Tarnovan, I.G. & Crisan, T.E. Radiation optimization and image processing algorithms in the identification of hand vein patterns. *Comput. Stand. Interface.*, 2010, **32**(3), 130-140. doi: 10.1016/j.csi.2009.11.008
17. Huang, D.; Tang, Y.; Wang, Y. & Chen, L. Hand vein recognition based on oriented gradient maps and local feature matching. *In Proceedings of the 11<sup>th</sup> Asian Conference on Computer Vision*. Verlag Berlin Heidelberg, 2012.
18. Wang, Y. & Liao, W. Hand vein recognition based on feature coding. *In Proceedings of the 7<sup>th</sup> Chinese conference on Biometric Recognition*. Guangzhou, China, 2012. doi: 10.1007/978-3-642-35136-5\_21
19. Wang, Y.; Li, K.; Shark, L.K. & Varley, MR. Hand-dorsa vein recognition based on coded and weighted partition local binary patterns, *In Proceedings of International Conference on Hand based Biometrics*. Hong Kong, China, 2012.
20. Premalatha, K.; Anantha Kumar, T. A. & Natarajan, A.M. A dorsal hand vein recognition-based on local gabor phase quantisation with whitening transformation. *Def. Sci. J.*, 2014, **64**(2), 159-167. doi: 10.14429/dsj.64.4659
21. Anantha kumar, T. & Premalatha, K. Personal identification using local Gaussian quadrature filter pair phase quantisation of hand vein images. *Int. J. Biometrics.*, 2014 **6**(2), 180-203.
22. Kannala, J. & Rahtu, E. Bsif: Binarised statistical image features. *In Proceeding of 21st International Conference on Pattern Recognition (ICPR)*, 2012, pp. 1363-1366.
23. Martin, A.; Doddington, G.R.; Kamm, t.; Ordowski, M. & Przybocki, M.A. The DET curve in assessment of detection task performance. *In the Proceedings of Eurospeech*. Rhodes, Greece, 1997.

## CONTRIBUTORS



**Mr T. Anantha Kumar** received his BE (Computer Science and Engineering) from Anna University, Chennai, in 2006 and ME (Computer Science and Engineering) from Anna University of Technology, Coimbatore, in 2009. He is currently working as a Senior Research Fellow for the DRDO sponsored project at Bannari Amman Institute of Technology, Erode, Tamil Nadu. His areas of interest include image processing, data mining and optimisation techniques.



**Dr K. Premalatha** is currently working as a Professor in the Department of Computer Science and Engineering at Bannari Amman Institute of Technology, Erode, Tamil Nadu. She did her PhD in Computer Science and Engineering (CSE) from Anna University, Chennai. Her research interests include data mining, image processing, information retrieval and soft computing.



**Dr A.M. Natarajan** is currently working as Chief Executive at Bannari Amman Institute of Technology, Erode, Tamil Nadu. He received BE, MSc and PhD from the PSG College of Technology, Coimbatore, India. He has more than 40 years of experience in Academic-Teaching, Research and Administration. He had published more than 70 papers in National and International Journals and has authored 10 Books. His research areas of interest include image processing, data mining, and soft computing.